metals

MDPI

Article

Experimental Study and Random Forest Machine Learning of Surface Roughness for a Typical Laser Powder Bed Fusion Al Alloy

Xuepeng Shan [1,2], Chaofeng Gao [2], Jeremy Heng Rao [2], Mujie Wu [1], Ming Yan [1,*] and Yunjie Bi [2,*]

[1] Department of Materials Science and Engineering, Southern University of Science and Technology, Shenzhen 518055, China; 12132031@mail.sustech.edu.cn (X.S.); 12112120@mail.sustech.edu.cn (M.W.)
[2] Ji Hua Laboratory, Institute of Advanced Additive Manufacturing, Foshan 528010, China; gaochf@jihualab.ac.cn (C.G.); raoheng@jihualab.com (J.H.R.)
* Correspondence: yanm@sustech.edu.cn (M.Y.); biyunjie@jihualab.com (Y.B.)

Abstract: Surface quality represents a critical challenge in additive manufacturing (AM), with surface roughness serving as a key parameter that influences this aspect. In the aerospace industry, the surface roughness of the aviation components is a very important parameter. In this study, a typical Al alloy, AlSi10Mg, was selected to study its surface roughness when using Laser Powder Bed Fusion (LPBF). Two Random Forest (RF) models were established to predict the upper surface roughness of printed samples based on laser power, laser scanning speed, and hatch distance. Through the study, it is found that a two-dimensional (2D) RF model is successful in predicting surface roughness values based on experimental data. The best and minimum surface roughness is 2.98 μm, which is the minimum known without remelting. More than two-thirds of the samples had a surface roughness of less than 7.7 μm. The maximum surface roughness is 11.28 μm. And the coefficient of determination (R^2) of the model was 0.9, also suggesting that the surface roughness of 3D-printed Al alloys can be predicted using ML approaches such as the RF model. This study helps to understand the relationship between printing parameters and surface roughness and helps print components with better surface quality.

Keywords: laser powder bed fusion (3D printing); surface quality; surface roughness; random forest; AlSi10Mg

Citation: Shan, X.; Gao, C.; Rao, J.H.; Wu, M.; Yan, M.; Bi, Y. Experimental Study and Random Forest Machine Learning of Surface Roughness for a Typical Laser Powder Bed Fusion Al Alloy. *Metals* **2024**, *14*, 1148. https://doi.org/10.3390/met14101148

Academic Editor: Chris Aldrich

Received: 24 August 2024
Revised: 4 October 2024
Accepted: 7 October 2024
Published: 8 October 2024

1. Introduction

Additive manufacturing (AM), more commonly known as 3D printing, is a novel processing approach distinct from traditional manufacturing. Compared to traditional machining, its processing method is more flexible and rapid, and it can achieve rapid printing and manufacturing without mold, thereby garnering considerable favor within industries. AM has been extensively utilized in aerospace, medical, and other domains [1]. Some automotive engineers are also studying how to replace conventional cast metal parts and stamped parts with parts produced by AM, which can help reduce mold costs, reduce upfront trial production costs, improve material utilization, and shorten production cycles [2].

Compared to traditional manufacturing, AM also has certain disadvantages. For instance, compared to traditional machining, the precision of the parts produced by AM is lower, which not only affects the quality of the parts themselves but also the assembly of different parts, strength, sealing performance, etc. of the entire system. Some characteristics of AM processing, such as the need to add a support structure during processing, will also affect its surface accuracy. An important parameter for measuring accuracy is surface roughness. Surface roughness refers to the micro-geometric characteristics composed of small spacing and peaks and valleys on the machined surface. It is a micro-geometric error,

also known as micro-unevenness. By using turning, grinding, and/or other processing methods, the surface roughness can be reduced to less than 0.01 μm [3]. The surface roughness of additively manufactured samples varies widely, ranging from 2 μm to 90 μm, which is mainly related to the process parameters used, the materials used, and the settings of the surface optimization parameters. In many kinds of additive manufacturing, Laser Powder Bed Fusion (L-PBF) has the lowest accuracy and the lowest surface roughness of the parts produced [4,5]. Gao et al. [6] have successfully reduced the surface roughness of Al-Si alloy parts printed by selective laser melting to 2 μm, which is the lowest known surface roughness of additively manufactured metal parts. Based on the results of their experiments, it was also noticed that the printing parameters are the most influential factors on the surface roughness of homogeneous metal parts.

To solve the specific relationship between the printing parameters and the surface roughness, artificial intelligence such as machine learning (ML) is preferred because too many variables are involved. ML is also capable of predicting based on obtained experimental results, where it represents the behavior of a computer that adapts its own computational aspects through experience gained from cyclic computing [7].

Several researchers have used ML models to predict the surface roughness of samples for AM. For instance, in order to predict the surface roughness of Ti-6Al-4V alloy samples printed by L-PBF, Fotovvati and Chou [8] studied the influence of various L-PBF process parameters on samples' surface roughness; their results show that laser power has the greatest influence on the surface roughness of a sample. Li et al. [9] predicted the surface roughness of as-printed polylactic acid fabricated from fused deposition modeling. Yang et al. [10] developed an artificial neural network model to predict the surface roughness of printed 316L stainless steel samples in order to predict and improve the surface quality. They investigated the ensemble machine learning models to predict the mechanical properties of the 3D-printed Polylactic Acid (PLA) specimens. Deb et al. [11] used a variety of ML methods to predict the tensile strength and surface roughness of 3D-printed PLA based on process parameters. The experimental results show that the surface roughness of printed samples can be improved by adjusting the process parameters. Chen et al. [12] propose a machine learning method based on Gaussian process regression to construct a model between the Wire Arc Additive Manufacturing (WAAM) process parameters and top surface roughness. Experimental results demonstrate that the proposed method achieves less than 50 μm accuracy in surface roughness prediction. Gogulamudi et al. [13], to study the surface roughness of L-PBF aluminum alloy, developed a model to predict the optimal process parameters for producing AlSi10Mg components with desired surface roughness and Vickers microhardness.

Existing research covers a variety of approaches to ML and AM. This brings some inspiration to our research, but at the same time, there are several problems. For example, the vast majority of studies print a small number of experimental samples, in most cases fewer than 100 samples. Moreover, the surface roughness of the printed samples in most experiments is too large, which means that the printed parts may have surface defects and thus affect the surface roughness. This creates noisy labels in the data. These factors affect the predictions of ML models. Therefore, this experiment increased the number of experimental samples and reduced the surface defects of samples by controlling the range of process parameters to improve the accuracy and generality of ML predictions.

There are various types of ML models. In order to make it easy to give a suitable formula for predicting the process parameters' effects on the surface roughness, Random Forest (RF) regression was selected to use in this study. RF is an integrated learning based on a decision tree algorithm. The decision trees approach is an important classification and regression method in data mining techniques [14], which is a predictive analytic model expressed in the form of binary and multinomial trees [15]. In the RF, each decision tree is independent and trained on a randomly selected subsample, which effectively reduces the risk of overfitting [16]. RF obtains the final regression results by averaging or weighted averaging the predictions of multiple decision trees [17]. Furthermore, according

to the different number of feature values corresponding to each set of data, RF can be classified into different categories, such as one-dimensional (1D) RF regression models, two-dimensional (2D) RF regression, and so on. Descriptors are vectors used to depict the features of the data, which are mainly used to help ML models understand the data features [18]. A model with one descriptor for a piece of data is a 1D RF model, and a model with two descriptors for a piece of data is a 2D RF model.

To sum up, the aim of this study is to discover the relationship between surface roughness and process parameters for L-PBF. To achieve this, several groups of experimental samples were printed, a database was constructed, a RF model was established to predict the surface roughness of the printed samples according to the printing parameters, and the regression equations of both were given. The typical alloy selected in this experiment is AlSi10Mg, which is one of the most commonly used alloys in L-PBF. Its surface quality, however, is relatively poor, and its surface roughness is high [19], which is because Al alloys tend to have low fluidity [20], high thermal conductivity, and high laser reflectivity [21]. Improvement of its surface roughness can enhance its surface quality and can help avoid the necessity and cost of subsequent machining. Compared with the existing experiments, the parameter setting range in this study is more reasonable, and there are more experimental data. Machine learning has a larger database and a lower noise value of the data. The prediction results are more accurate and reasonable.

2. Experimental

2.1. Materials and Methods

The instrument used for printing was an FS273M printer (Farsoon Technologies, Changsha, China), and the surface roughness instrument used for the experiment was the Surftest SJ-310 measuring instrument (Mitutoyo, Suzhou, China). Each sample was measured three times, with each measurement taken at a distance of 0.8 μm. The three measurement lines and the edge of the sample were parallel to each other. Measurement lines 1 and 3 were 2 mm from the edge, respectively, and measurement line 2 was located in the center of the sample. In the process of measurement, some references were made to reduce measurement errors. [22,23] The surface profile of some samples was measured by the Countor GT K 3D profiler (Bruker, Berlin, Germany). Laser energy density, B, was used to describe the overall experimental parameters, as shown in the following formula (Equation (1)) [4]:

$$B = \frac{P}{vth} \tag{1}$$

where P is the laser power (W), v is the scanning speed (mm/s), h is the hatch distance (μm), and t is the layer thickness (μm).

During the printing process, both too low and too high energy densities increase the surface roughness during printing. If the energy density is too low, it may lead to incomplete melting of the powder and make defects on the surface of the sample; if the energy density is too high, it may lead to splashing of the liquid metal and affect the surface roughness of the part [24,25]. The selected experimental variables were laser power, laser scanning speed, and hatch distance; see Table 1. The basic parameters were the commonly used AlSi10Mg printing parameters provided by the printer equipment manufacturer. On this basis, the research articles on AlSi10Mg should be referred to [26,27]. The range of parameter variation was given. In the experiment, the process parameters of sample 1 were set as the basic parameters, and the remaining sample parameters were determined by random selection. There was no replication of experimental data. Since the thickness of the powder layer cannot be adjusted during printing, we have standardized the powder layer thickness for all parts to 30 μm, as this is the most commonly used thickness for this aluminum alloy. For printing, the sample placement is shown in the following figure (Figure 1). A total of 144 different sets of experimental samples were designed. The samples were rectangles 1.2 cm in width by 1 cm in height. We conducted all sample prints at once, set all parts to the same scanning strategy, and eliminated the remelting process to minimize

the influence of extraneous factors. Furthermore, the chosen printer was equipped with a dynamic focusing function that mitigates deviations in the laser incidence angle caused by varying positions of components on the substrate.

Table 1. Printing parameters were used in this study.

Parameter	Basic Parameter	Range of Variable
Laser power	340 W	270~420 W
Laser scanning speed	1100 mm/s	800~1400 mm/s
Hatch distance	0.15 μm	0.08~0.16 μm

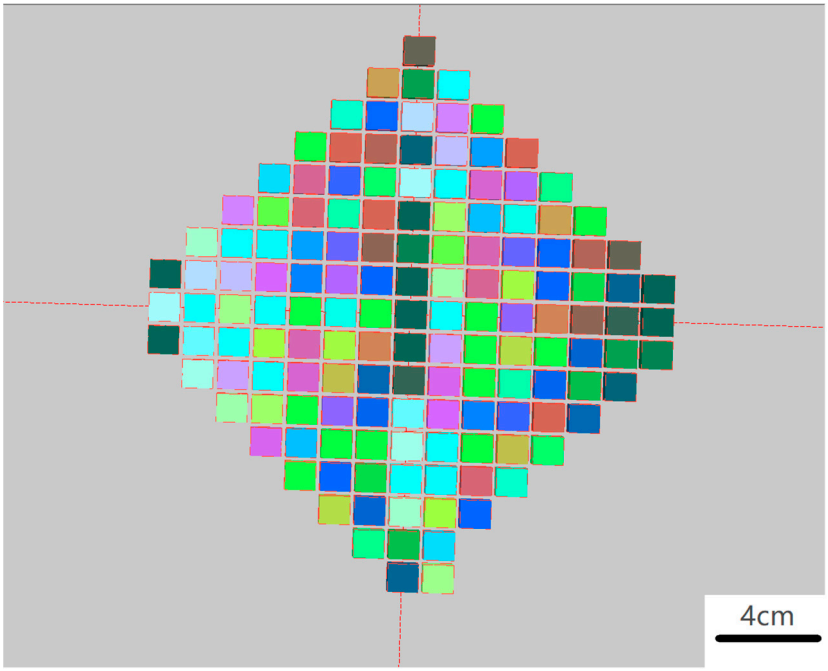

Figure 1. The way the samples were placed during printing.

2.2. Random Forest Regression

As mentioned above, the RF regression is an algorithm based on bootstrap aggregation (bagging). Multiple decision trees are predicted in parallel, and the average predicted value of all decision trees is ultimately given [28]. The operation principle is also shown in Figure 2.

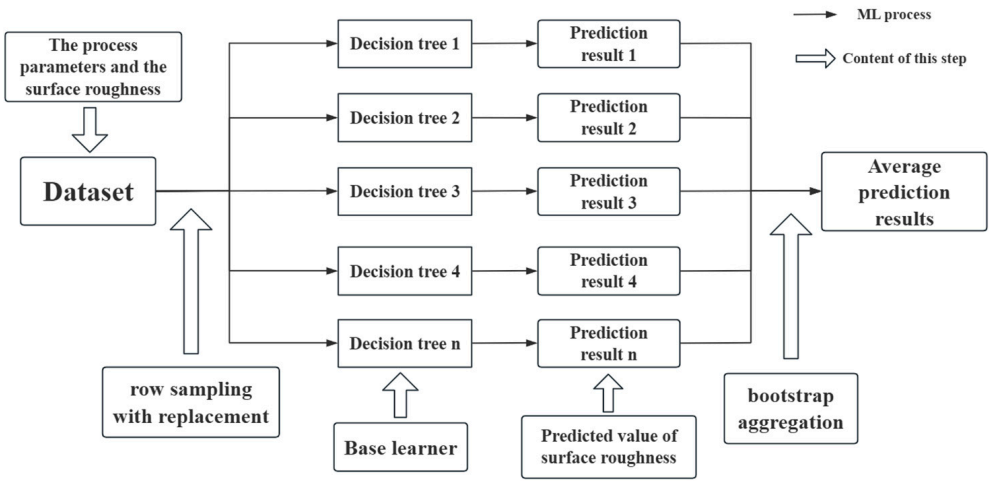

Figure 2. Development procedure for the RF regression model.

The RF model randomly extracts multiple samples from the original data set and generates multiple subsets of data. For each subset of data, a regression tree is constructed using the decision tree algorithm. When each node splits, some features are randomly selected, and the best features (laser power, laser scanning speed, and hatch distance) are selected for splitting. After all trees are trained, each decision tree is used to predict the newly input data points, and then all the predicted results are averaged to obtain the final predicted value. The equations for the RF model are as follows (Equation (2)) [29]:

$$y = \frac{1}{N}\sum_{n=1}^{N} y_n \quad (2)$$

where y is the average prediction result, N is the number of decision trees, and y_n is the prediction result given by n-numbered decision trees (1 < n < N). The specific process of each tree in the experiment is shown in Figure 3.

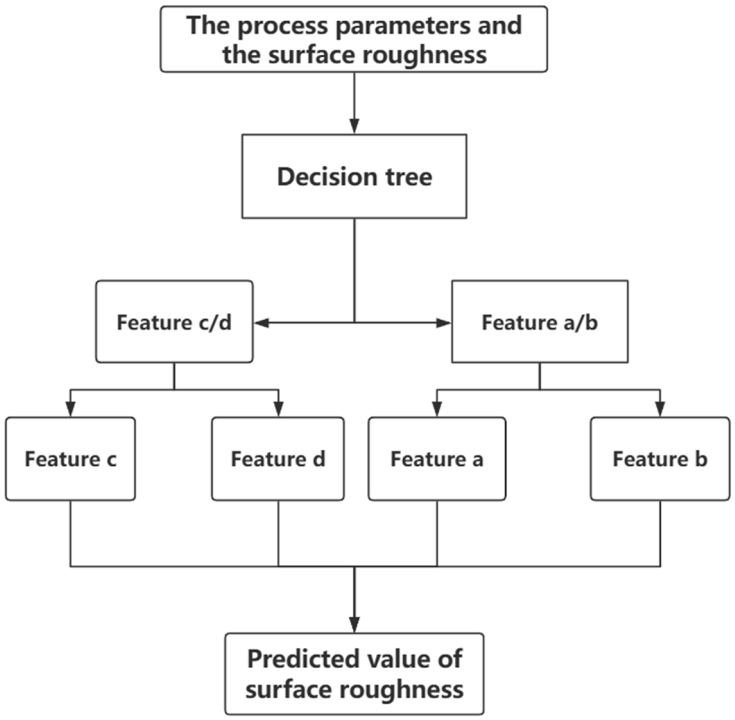

Figure 3. Decision tree prediction process.

After the prediction result is obtained, the regression equation can be obtained by non-linear regression according to the split way of the decision tree. The regression method is the least squares method. The equation for the least squares method is expressed as follows (Equation (3)) [7]:

$$min\sum_{i=1}^{n} w|y_i - \hat{y}_i|^2 \quad (3)$$

where y_i denotes the true observation, $\hat{y}_i$ denotes the predicted value, w denotes precision, and n denotes the number of decision trees.

In this experiment, there were 144 sets of data in total, where the eigenvalues were the printing parameters, and the three eigenvalues were the laser power, scanning speed, and scanning spacing. The target variable was surface roughness. For a better regression, a part of the data with a large noise value was removed, and the remaining data was set up as a database. The number of decision trees was set to 1000. The depth of each tree was set to 0. A 1D RF regression model and a 2D RF regression model were chosen to compare the regression equations and prediction accuracy given by the two models. The software used in this experiment was Anaconda (version 2.3.2). An RF model was built in Python (version 3.7.0).

The method of obtaining the regression equation was the standard equation method, which aims to obtain the parameter θ that minimizes the value of the cost function. The cost function formula was as follows:

To determine the prediction accuracy, some parameters, namely the mean square error (MSE), root mean square error (RMSE), mean absolute error (MAE), and determination coefficient (R^2), were used, and they are described below [11].

The formula for R^2 is as follows (Equation (4)):

$$R^2 = 1 - \frac{\sum_{i=1}^{n}(y_i - \hat{y}_i)^2}{\sum_{i=1}^{n}(y_i - \overline{y})^2} \quad (4)$$

where y_i denotes the true observation, $\hat{y}_i$ denotes the predicted value, $\overline{y}$ denotes the mean of the true observation, and n denotes the number of observations.

The formulas for MSE and RMSE are as follows (Equations (5) and (6)):

$$MSE = \frac{1}{n}\sum_{i=1}^{n}(y_i - \hat{y}_i)^2 \quad (5)$$

$$RMSE = \sqrt{\frac{1}{n}\sum_{i=1}^{n}(y_i - \hat{y}_i)^2} \quad (6)$$

where y_i denotes the true observation, $\hat{y}_i$ denotes the predicted value, and n denotes the number of observations.

The equation for MAE is expressed as follows (Equation (7)):

$$MAE = \frac{1}{n}\sum_{i=1}^{n} \mid y_i - \hat{y}_i \mid \quad (7)$$

where y_i denotes the true observation, $\hat{y}_i$ denotes the predicted value, and n denotes the number of observations.

3. Results

3.1. Experimental Result

The surface morphology and surface roughness of the printed parts were measured. The surface morphology of some parts was shown in Figure 4.

It can be seen from the surface profiles of some extracted samples that the surface profiles of the samples are relatively smooth, without major surface defects, and will not affect the measurement of surface roughness.

The printing parameters of the experimental samples were set in Table 2. After printing, the surface roughness values of all samples were measured and organized into a histogram (Figure 5). From the histogram, it can be seen that the surface roughness values ranged from 2.90 μm to 11.30 μm. Most of the samples had surface roughness values clustered between 4.10 μm and 7.70 μm. We set the lower limit at 2.9 μm and the upper limit at 11.3 μm, dividing the range into seven equal intervals, each with a width of 1.2 μm. The printing parameters of the five best samples are organized in Table 3, and the rest of the data are included in Appendix A.

Two points can be found in Table 3: Firstly, the energy density of several points with the lowest roughness is very high, e.g., ~130–150 J/mm^3. Secondly, the best hatch distance is around 0.12 μm. This means that a combination of high laser power, low scanning speed, high laser energy density, and suitable hatch distance can reduce the surface roughness of the printed AlSi10Mg samples.

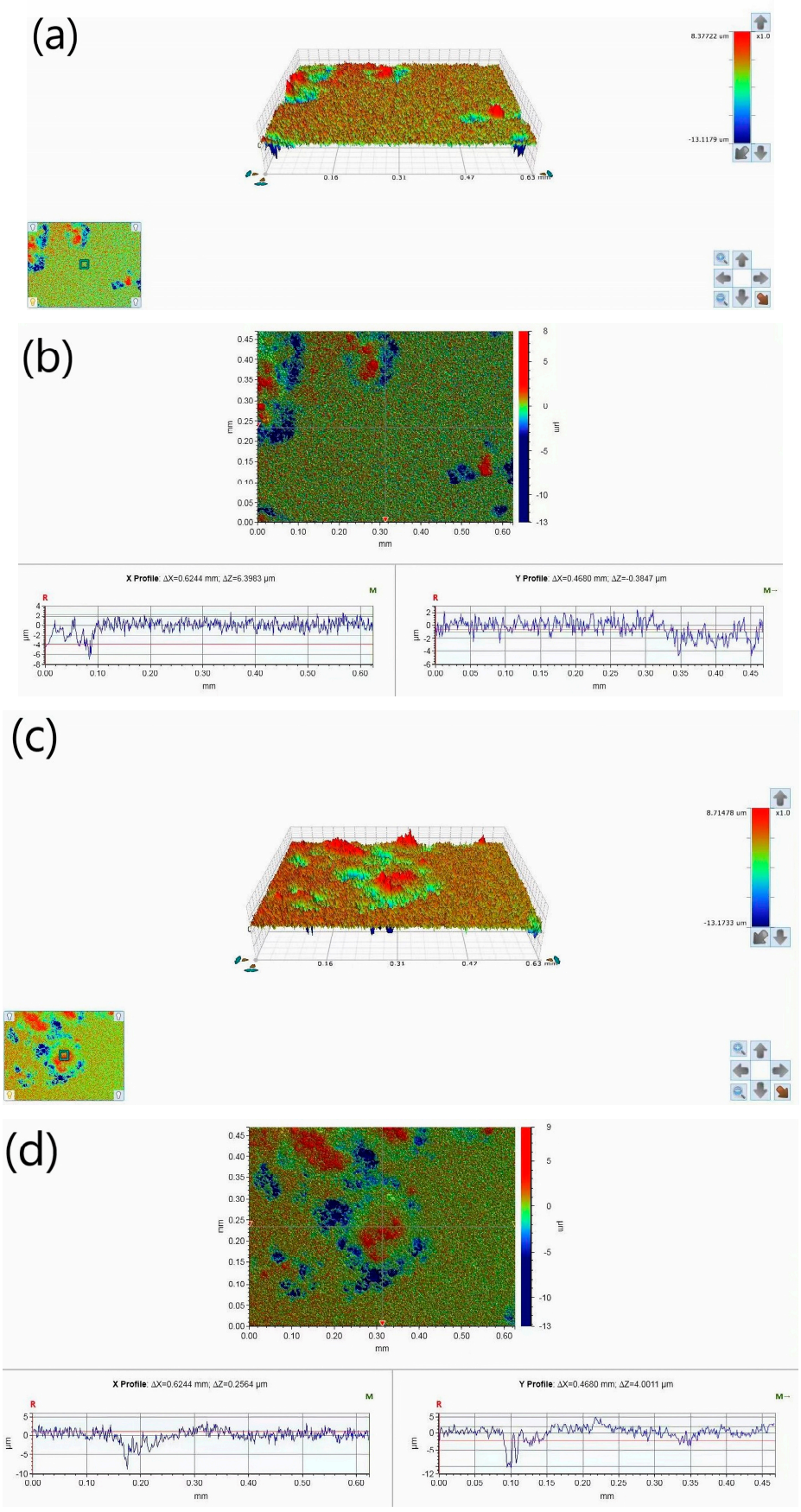

Figure 4. Surface profiles of the experimental samples: (**a**,**b**) show the surface profile of sample 1; (**c**,**d**) show the surface profile of sample 2.

Table 2. Process parameters of the samples (part).

Sample Number	Laser Power (W)	Laser Scanning Speed (mm/s)	Hatch Distance (μm)	Laser Energy Density (J/mm^3)
1	340	1100	0.15	68.7
2	325	1251	0.08	108.2
3	321	1281	0.15	55.7
4	348	1091	0.14	75.9
5	343	1176	0.08	121.5
6	375	1330	0.08	117.5
7	399	917	0.11	131.9
8	398	912	0.16	90.9
9	317	810	0.13	100.3
10	292	882	0.12	92
11	411	938	0.09	162.3
12	330	1239	0.12	74
13	354	1050	0.15	74.9
14	360	927	0.12	107.9
15	330	887	0.08	155
16	366	1172	0.16	65.1
17	270	1128	0.12	66.5
18	288	869	0.12	92.1
19	343	1047	0.12	91
20	328	1382	0.1	79.1
...	...	...	...	...

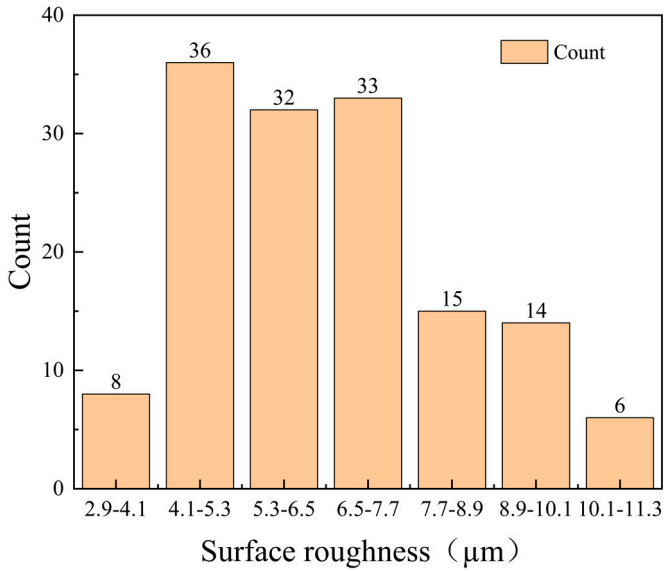

Figure 5. Surface roughness histogram.

Table 3. The best printing parameters and corresponding surface roughness (see Appendix Table A1 for the complete table).

Sample Number	Surface Roughness (μm)	Laser Power (W)	Laser Scanning Speed (mm/s)	Hatch Distance (μm)	Laser Energy Density (J/mm^3)
14	3.26	360	927	0.12	107.9
26	3.95	395	1073	0.13	94.4
44	3.15	414	861	0.12	133.6
48	3.76	414	1079	0.09	142.1
116	2.98	415	917	0.1	150.9

To further compare the relationship between surface roughness and laser energy density, the corresponding laser energy density and surface roughness of all 144 samples were counted and prepared as a scatter plot (Figure 6). The R^2 for this linear fit is 0.22. It can be seen from the figure that the laser energy density is indeed inversely proportional to the surface roughness as a whole, and the higher the laser energy density, the lower the surface roughness of the sample. The relationship between them is weakly and inversely correlated. However, the relationship between laser energy density and surface roughness is very complex, so this part is only a simple reasoning of the relationship between the two. The relationship between process parameters, laser energy density, and surface roughness also needs to be inferred from the ML prediction results.

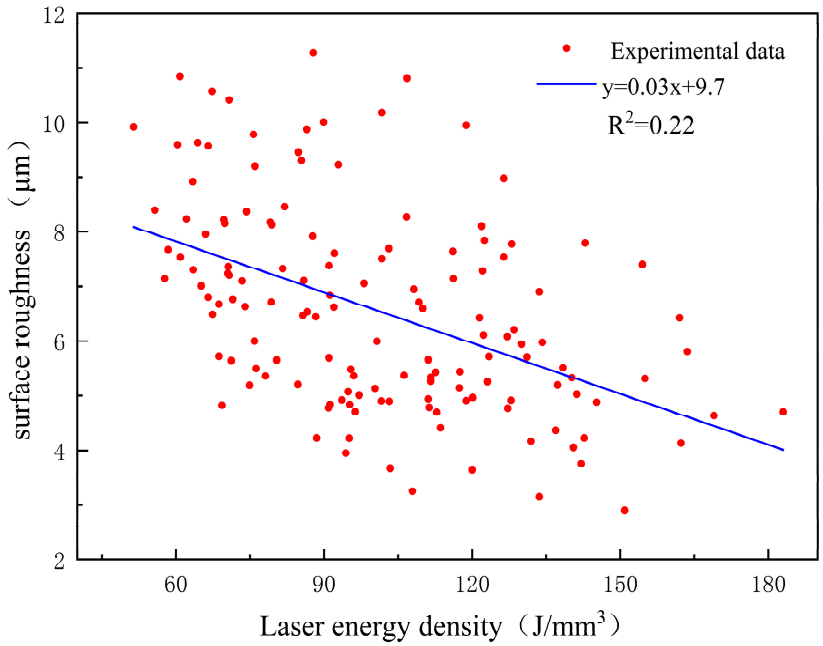

Figure 6. Scatter plot for surface roughness–laser energy density.

Meanwhile, from the corresponding linear fitting, some data distribution is relatively discrete. This is most likely because of uncontrollable factors during the printing process. For example, the airflow field can impact the roughness of the printed parts [30]. The printer's blower device can blow up fine spray powder during printing, which may splash onto other nearby sample surfaces, affecting surface forming and roughness. The surface roughness of individual samples fluctuates within a range of 1–2 μm, making predictions challenging when the surface roughness is excessively low. This leads to training data that is noisy, which affects the prediction results of the model [31]. To reduce errors in the regression prediction and improve the accuracy of the machine learning model, data that are too discrete are removed, and the remaining data are used as a database for the following ML regression.

3.2. Prediction Results and Regression Equations of the RF Regression Model (1D)

A 1D RF prediction model was run with a corresponding descriptor for each eigenvalue. The model is used to predict the training set and test set, respectively. The training set is used to estimate the parameters in the model so that the model reflects reality, while the test set is used to evaluate the predictive performance of the model. The comparison table between the predicted value and the real value is also sorted out, and part of the data are shown in Table 4.

Table 4. Random Forest Regression (1D) prediction results (part).

Sample Number	Surface Roughness (μm)	Predicted Value (μm)	Error (%)	Descriptor
1	5.72	6.65	16%	3.45×10^{-3}
2	6.95	7.86	13%	4.15×10^{-3}
3	8.40	8.15	3%	4.31×10^{-3}
4	6.00	6.35	6%	3.28×10^{-3}
5	6.42	6.89	7%	3.59×10^{-3}
6	5.44	6.51	20%	3.38×10^{-3}
7	4.17	4.25	2%	2.09×10^{-3}
8	4.78	4.25	11%	2.08×10^{-3}
9	5.13	5.78	13%	2.96×10^{-3}
10	6.62	7.23	9%	3.79×10^{-3}
11	4.14	4.11	1%	2.01×10^{-3}
12	6.63	7.62	15%	4.01×10^{-3}
13	5.19	5.98	15%	3.07×10^{-3}
14	3.26	5.20	60%	2.63×10^{-3}
15	5.32	5.84	10%	3.00×10^{-3}
16	7.01	6.17	12%	3.18×10^{-3}
17	9.57	9.87	3%	5.30×10^{-3}
18	7.61	7.31	4%	3.83×10^{-3}
19	5.69	6.30	11%	3.25×10^{-3}
20	8.18	8.28	1%	4.38×10^{-3}
…	…	…	…	…

In the regression, the first 100 sets of data are used as the test set, and the last 20 sets of data are used as the training set. The data, including the real values and predicted values, as well as the corresponding eigenvalue of each data, are included in Appendix Table A2 The predicted and true values given by the model were sorted into graphs for the training set and the test set, respectively (Figure 7).

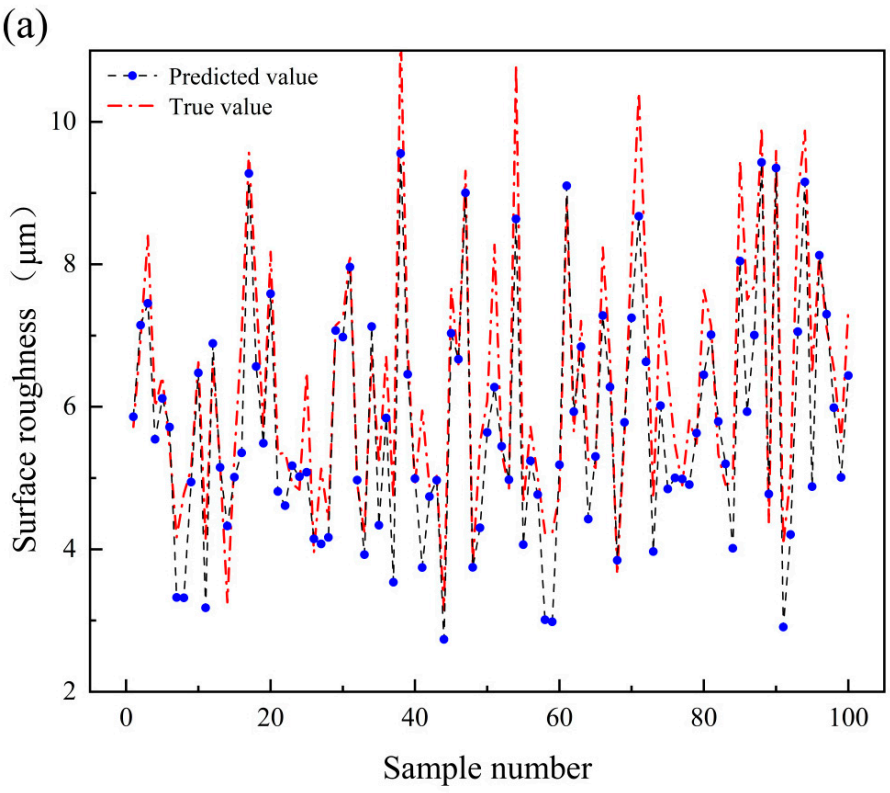

Figure 7. *Cont.*

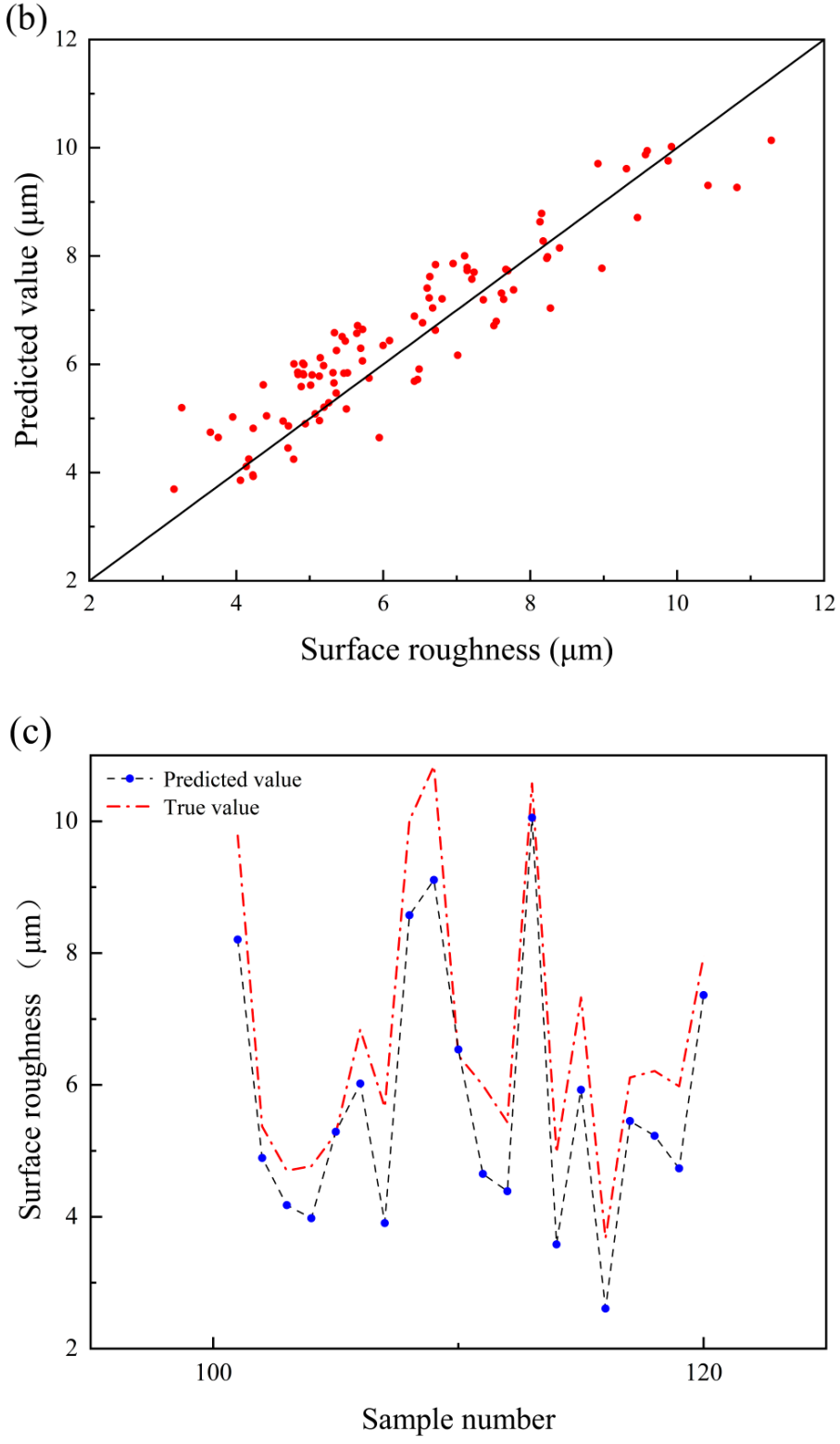

Figure 7. *Cont.*

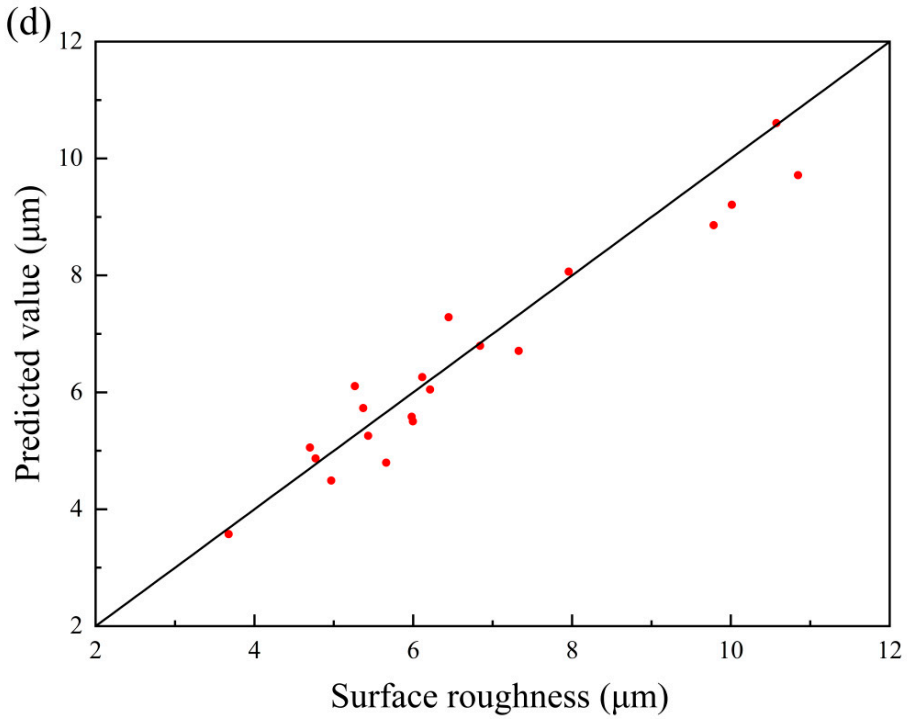

Figure 7. Comparison of the surface roughness prediction results given by one-dimensional Random Forest Regression: (**a**,**b**) are the predicted surface roughness values and the real observed values in the training set; (**c**,**d**) are the predicted surface roughness values and the real observed values in the test set.

The formula for the regressed surface roughness, R, is as follows (Equation (8)):

$$R = \ln\left(\frac{1752.6a}{b^2}\right) + 0.6 \tag{8}$$

where a is the laser scanning speed (mm/s), and b is the laser power (W). The image of the equation is shown in Figure 8. According to the established equation, the surface roughness is proportional to laser scanning speed and inversely proportional to laser power, suggesting that the higher the laser power, the lower the scanning speed, the lower the surface roughness, and the better the surface performance of the printed sample. This is consistent with previous experimental findings that surface roughness is inversely proportional to laser energy density.

The regression equation does not contain all the features, which indicates that there are some problems in the pruning process of the decision tree, resulting in a lack of features. To solve this phenomenon, it is necessary to add data descriptors so that the RF model can understand the data more accurately and make the model more complex to avoid the influence of single decision tree pruning errors.

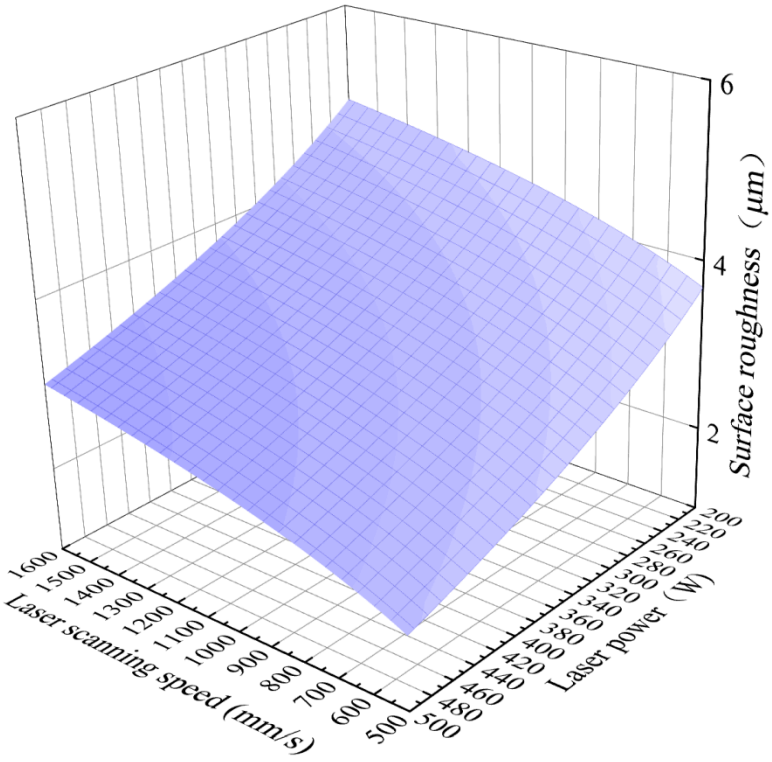

Figure 8. Regression equation of the surface roughness using the 1D RF model.

3.3. Prediction Results and Regression Equations of Random Forest Regression Model (2D)

Table 5 compares some of the experimental and predicted values in the 2D RF model. The complete data of the samples, as well as the eigenvalues corresponding to each data point, are listed in Appendix Table A3.

Table 5. Random Forest Regression (2D) prediction results (part).

Sample Number	Surface Roughness (μm)	Predicted Value (μm)	Error (%)	Descriptor 1	Descriptor 2
1	5.72	6.25	9%	2.14×10^1	-3.76×10^2
2	6.95	7.80	12%	2.06×10^1	-2.09×10^2
3	8.40	7.88	6%	2.12×10^1	-3.92×10^2
4	6.00	5.91	1%	2.14×10^1	-3.66×10^2
5	6.42	6.73	5%	2.08×10^1	-2.18×10^2
6	5.44	6.29	16%	2.12×10^1	-3.05×10^2
7	4.17	3.81	9%	2.17×10^1	-3.48×10^2
8	4.78	4.53	5%	2.21×10^1	-4.99×10^2
9	5.13	5.60	9%	2.10×10^1	-2.10×10^2
10	6.62	7.50	8%	2.06×10^1	-1.86×10^2
11	4.14	3.82	8%	2.17×10^1	-3.23×10^2
12	6.63	7.17	8%	2.11×10^1	-3.19×10^2
13	5.19	5.60	20%	2.16×10^1	-3.92×10^2
14	7.01	6.57	6%	2.18×10^1	-5.05×10^2
15	9.56	9.84	3%	2.03×10^1	-2.14×10^2
16	7.60	7.70	1%	2.05×10^1	-1.79×10^2
17	5.69	5.75	1%	2.12×10^1	-2.92×10^2
18	8.17	7.88	4%	2.09×10^1	-2.94×10^2
19	5.33	5.33	0%	2.12×10^1	-2.61×10^2
20	5.359	5.55	4%	2.18×10^1	-4.64×10^2
...	...	...	...	...	...

Furthermore, the predicted values and experimental values given by the model on the training set and the test set were organized into line plots and scatter plots, respectively, see Figure 9.

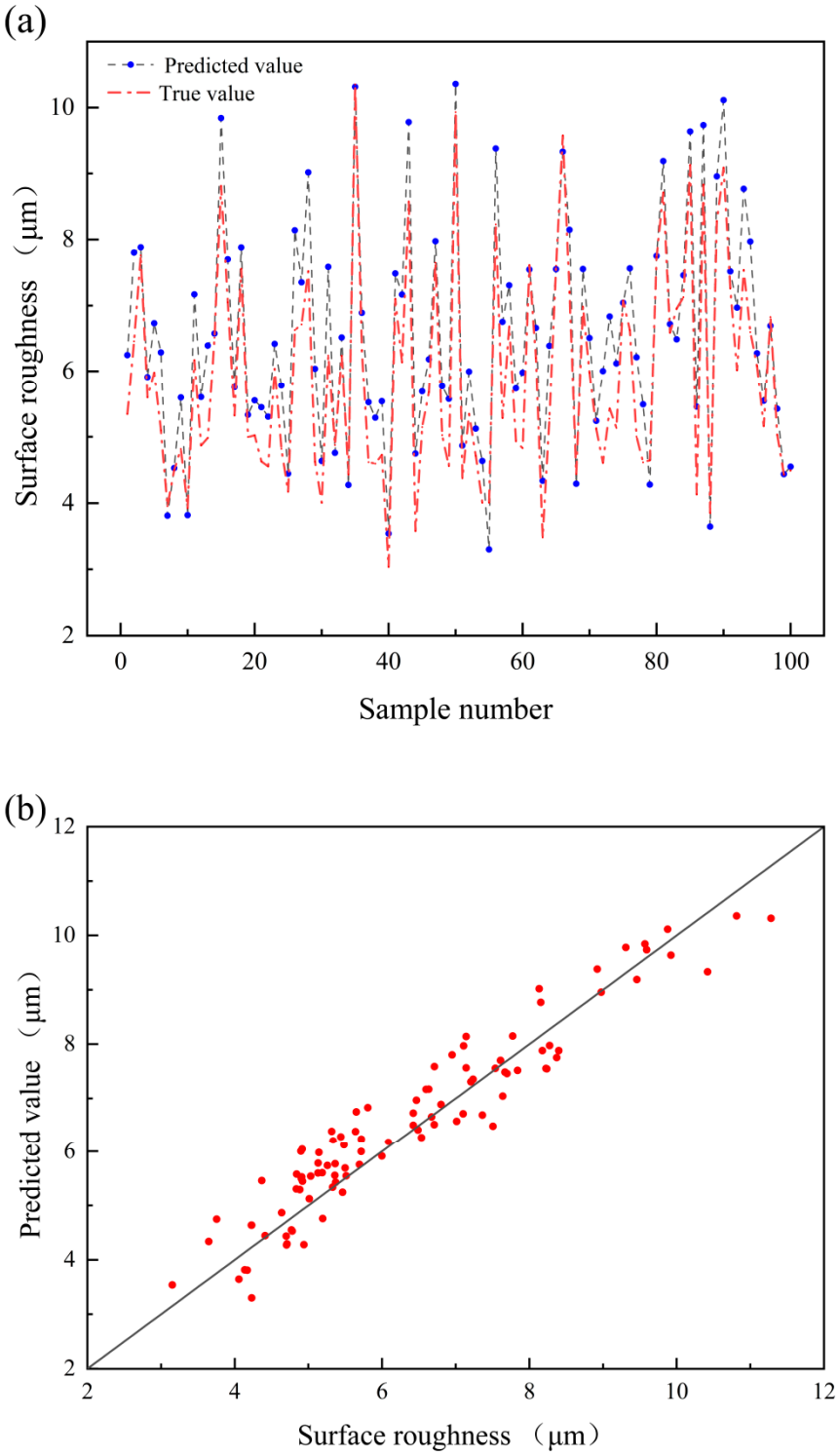

Figure 9. *Cont.*

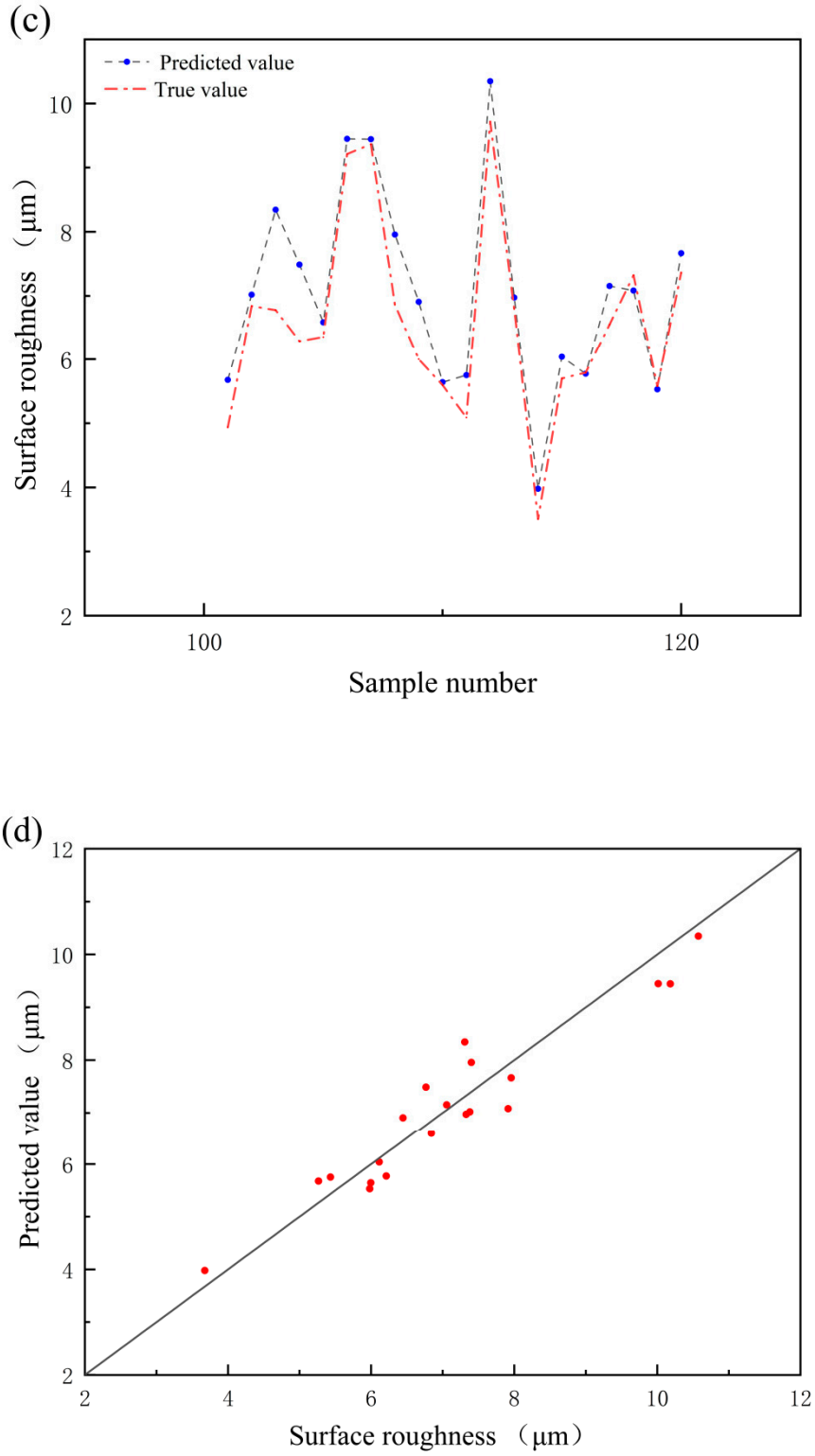

Figure 9. Comparison of surface roughness prediction results given by 2D RF: (**a**,**b**) are the predicted surface roughness values for the training set; (**c**,**d**) are the predicted surface roughness values for the test set.

The regressed surface roughness, R, using the 2D RF model is as follows (Equation (9)):

$$R = -5.786 \ln\left(\frac{b^4}{c}\right) + \frac{0.0187ac}{\sin(\ln b)} + 141.138 \quad (9)$$

where a is the laser scanning speed (mm/s), b is the laser power (W), and c is the hatch distance (μm). It can be seen that the regression equation given by the 2D RF regression model is different from that of the 1D model. Since there are three variables in this regression equation, it is not possible to draw the function diagram directly. After setting the hatch distance to 0.01 μm, the function diagram is presented in Figure 10.

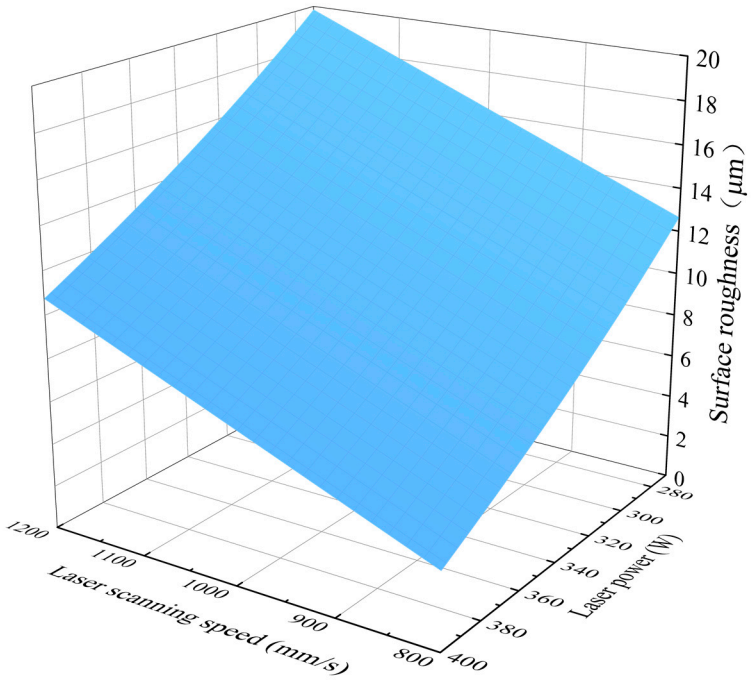

Figure 10. Regression equation of the surface roughness using the RF 2D model.

By checking the regression equation, it can be found that the value of $\sin(\ln b)$ in the equation has a small change (0.097–0.105) in the laser power range (270 W–420 W) given in this experiment, which can be regarded as a constant. Based on this, the surface roughness of the printed samples shows a tendency of decreasing with the increase in laser power and increasing with the increase in laser scanning speed, while the relationship between the surface roughness and the hatch distance depends on the specific parameters.

4. Discussion

By comparing the prediction accuracy of the two different models, the reference coefficients for the 1D and 2D RF models are sorted in Table 6. From the table, it can be seen that, in comparison, the 2D RF regression model has lower values of MSE, RMSE, and MAE, and its R^2 is closer to 1. All four evaluation parameters are better than the 1D RF regression model, indicating that the 2D RF regression model gives a more accurate prediction.

Table 6. Comparison of evaluation parameters between the 1D model and 2D model.

Evaluation Parameter	R^2	MSE	RMSE	MAE
Argument (1D model)	0.865	0.350	0.592	0.582
Argument (2D model)	0.907	0.255	0.505	0.464

Based on the regression equations obtained above, it was found that the two equations have similar resulting images and patterns of change, but the regression equation given by the 2D RF regression model includes the variable of hatch distance. This is because by adding a descriptor, the ML process learns more features, which helps understand the relationship between the input features and the real observations. A more reasonable regression equation is therefore realized by the 2D RF regression; also, the regression

equation given by the 2D RF regression model contains all the eigenvalue variables. Based on the 2D RF regression equation, it can be observed that surface roughness decreases as laser power increases and increases as scanning speed increases. Additionally, the relationship between surface roughness and hatch distance varies based on the specific value of the hatch distance. Similar patterns can also be derived from the 1D RF regression equation. As laser power increases, scanning speed decreases, leading to an increase in laser energy density and a decrease in surface roughness. The conclusion aligns with our findings at the end of Chapter 3.1. However, it is important to note that this conclusion may not hold true when the process parameters fall outside the range specified in this experiment. Additionally, the surface roughness could be impacted by uncontrollable external factors, leading to a small margin of error. By further comparing the results of this study with previous studies (Table 7), it is evident that our results are among the best ones, achieving a minimum surface roughness of below 3 μm [6,13]. The experimental results show that surface defects have less impact, leading to more accurate predictions. Additionally, the machine learning database used in this study is larger, allowing for a wider range of predictions. This experiment also obtained regression equations for AlSi10Mg surface roughness and process parameters, a first in known research. This contributes to a better understanding of the relationship between surface roughness and process parameters.

Table 7. Surface roughness results obtained in this study and other references [4,23].

	Reference Study	**Our Study**
Minimum surface roughness	2.5 μm [6] 8.67 μm [13]	2.95 μm
Machine learning model	Deep learning [13]	Random forest
Regression equation	Excluded	Contained

5. Conclusions and Outlook

5.1. Conclusions

The main results obtained in this study are summarized as follows:

(1) In order to study the correlation between the surface roughness of a typical Al alloy and the printing parameters, experiments were designed in which a total of 144 sets of samples were printed to study changes in surface roughness under the influence of key printing parameters. The lowest surface roughness achieved was 2.95 μm, indicating that it is possible to print Al alloys with a good surface quality by process optimization without using remelting.

(2) Based on the obtained experimental data, Random Forest regression was built to regress and predict the results. After optimizing the model, a 2D prediction model was developed with high prediction accuracy. The R^2 of the model is 0.907, with an MSE of 0.255, RMSE of 0.505, and MAE of 0.464. The specific relationship equation between the key printing parameters and surface roughness was also derived. A 2D RF model can maintain high prediction accuracy on both the training set and test set. The experimental parameters in the training set and test set cover the range of printing parameters of AlSi10Mg. This proves that the obtained ML model can provide accurate prediction results for the indicated roughness study of the aluminum alloy.

5.2. Outlook

In comparison to existing experimental results, this experiment collected a larger amount of data, with a total of 144 groups of experimental data being designed. The surface roughness of the samples was also lower. The experiment used the common printing parameter interval for AlSi10Mg. The average prediction error was less than 0.5 μm, indicating higher prediction accuracy across a wider range of applications. The regression equation between process parameters and surface roughness was also proposed in this experiment, which helps us to understand the relationship between the two. However,

there are some drawbacks to this experiment. Even though the data set used for machine learning in this experiment was already much larger than the data set in the existing research results, to predict the results more accurately, it is still necessary to build a data set containing more experimental data. If a data set of more than a thousand printed parts can be included, then the prediction accuracy of the model will surpass all known results.

Author Contributions: Conceptualization, X.S. and C.G.; methodology, X.S. and C.G.; software, X.S.; validation, X.S.; formal analysis, X.S.; investigation, J.H.R. and M.W.; resources, C.G., J.H.R., M.Y., and Y.B.; data curation, M.W.; writing—original draft, X.S.; writing—review and editing, M.Y.; visualization, X.S.; supervision, M.Y. and Y.B.; project administration, Y.B. All authors have read and agreed to the published version of the manuscript.

Funding: This work is supported by the Guangdong Basic Applied Basic Research Foundation, China (2023B1515120100), the Key Research and Development Program of Jiangsu Province (K22251901), the National Natural Science Foundation of China (52271032), and the Shenzhen Science and Technology Innovation Commission (JCYJ20220818100612027). The authors would also like to acknowledge the technical support of SUSTech CRF.

Data Availability Statement: The original contributions presented in the study are included in the article, further inquiries can be directed to the corresponding author.

Conflicts of Interest: The authors declare no conflict of interest.

Appendix A

Table A1. Process parameters and surface roughness of the printed sample.

Sample Number	Laser Power (W)	Laser Scanning Speed (mm/s)	Hatch Distance (μm)	Surface Roughness (μm)
1	340	1100	0.15	5.72
2	325	1251	0.08	6.95
3	321	1281	0.15	8.40
4	348	1091	0.14	6.00
5	343	1176	0.08	6.42
6	375	1330	0.08	5.44
7	399	917	0.11	4.17
8	398	912	0.16	4.78
9	317	810	0.13	5.13
10	292	882	0.12	6.62
11	411	938	0.09	4.14
12	330	1239	0.12	6.63
13	354	1050	0.15	5.19
14	360	927	0.12	3.26
15	330	887	0.08	5.32
16	366	1172	0.16	7.01
17	270	1128	0.12	9.57
18	288	869	0.12	7.61
19	343	1047	0.12	5.69
20	328	1382	0.1	8.18
21	377	1120	0.08	5.33
22	376	1070	0.15	5.36
23	353	1048	0.12	4.92
24	357	1042	0.12	4.84
25	372	1150	0.16	6.49
26	395	1073	0.13	3.95
27	409	1133	0.12	5.13
28	352	861	0.12	4.41
29	311	1115	0.08	7.14
30	300	1013	0.14	7.24

Table A1. *Cont.*

Sample Number	Laser Power (W)	Laser Scanning Speed (mm/s)	Hatch Distance (μm)	Surface Roughness (μm)
31	273	955	0.12	8.13
32	322	839	0.1	4.92
33	382	959	0.15	4.23
34	303	1061	0.12	6.71
35	377	1017	0.09	5.20
36	324	989	0.1	6.71
37	374	852	0.08	4.70
38	286	1358	0.08	11.28
39	338	1211	0.14	6.80
40	381	1188	0.09	4.91
41	408	1048	0.1	5.95
42	370	1062	0.08	4.88
43	364	1074	0.08	5.03
44	414	861	0.12	3.15
45	327	1244	0.15	7.67
46	343	1302	0.08	6.60
47	285	1236	0.09	9.31
48	414	1079	0.09	3.76
49	385	1053	0.16	5.50
50	356	1167	0.08	6.09
51	284	807	0.11	8.28
52	356	1124	0.11	5.36
53	374	1139	0.12	4.84
54	275	1073	0.08	10.81
55	363	895	0.08	4.64
56	390	1317	0.08	5.72
57	367	1050	0.12	5.01
58	409	896	0.16	4.23
59	396	841	0.11	4.23
60	403	854	0.12	5.71
61	355	1063	0.1	4.78
62	284	1244	0.12	8.92
63	291	804	0.15	5.65
64	343	1345	0.12	7.20
65	411	1236	0.09	5.26
66	331	940	0.1	5.14
67	302	1080	0.15	8.24
68	338	1172	0.14	6.67
69	391	987	0.11	3.65
70	354	1184	0.14	5.64
71	329	1311	0.12	8.22
72	285	983	0.15	9.63
73	275	1079	0.12	10.42
74	305	993	0.08	7.77
75	372	920	0.14	4.71
76	304	891	0.09	7.54
77	325	836	0.08	6.42
78	343	957	0.15	5.47
79	393	1269	0.1	4.90
80	318	810	0.08	5.81
81	321	935	0.12	5.48
82	339	1217	0.08	7.64
83	331	1275	0.15	7.14
84	351	1165	0.09	5.34
85	353	1053	0.11	4.91
86	373	933	0.12	4.94
87	397	1370	0.13	8.37

Table A1. *Cont.*

Sample Number	Laser Power (W)	Laser Scanning Speed (mm/s)	Hatch Distance (μm)	Surface Roughness (μm)
88	275	983	0.11	9.46
89	391	1184	0.15	7.10
90	370	1347	0.09	7.51
91	343	1386	0.08	7.70
92	272	1175	0.15	9.92
93	347	939	0.09	4.37
94	271	1151	0.13	9.59
95	413	891	0.11	4.06
96	419	1226	0.12	5.07
97	291	959	0.08	8.98
98	278	1190	0.09	9.88
99	335	868	0.09	7.79
100	295	803	0.1	7.84
101	402	1303	0.12	6.47
102	278	1020	0.13	8.15
103	298	1051	0.11	7.11
104	331	1062	0.12	6.54
105	368	1108	0.08	5.51
106	404	1318	0.11	9.23
107	323	1090	0.14	7.36
108	294	1177	0.11	9.78
109	328	858	0.12	5.37
110	354	872	0.12	4.70
111	395	1035	0.1	4.77
112	334	1142	0.08	8.11
113	378	1147	0.09	7.29
114	348	1040	0.1	5.26
115	405	1348	0.11	7.38
116	415	917	0.1	2.90
117	300	1368	0.12	7.54
118	317	1387	0.12	7.31
119	324	1259	0.12	6.77
120	335	836	0.1	6.91
121	366	1337	0.1	6.84
122	382	955	0.14	5.66
123	353	1132	0.15	4.83
124	330	1083	0.12	5.20
125	288	1187	0.09	10.01
126	316	1155	0.12	9.21
127	281	1023	0.09	10.18
128	292	1335	0.12	10.85
129	300	809	0.08	7.40
130	323	1109	0.11	6.45
131	393	1182	0.11	6.00
132	408	1208	0.1	5.43
133	280	1387	0.1	10.57
134	377	872	0.12	4.97
135	376	1396	0.11	7.33
136	359	1259	0.08	9.95
137	412	830	0.16	3.67
138	379	1291	0.08	6.11
139	378	1226	0.08	6.21
140	411	1396	0.1	7.06
141	285	828	0.14	8.46
142	408	1292	0.12	7.92
143	398	1236	0.08	5.98
144	328	1328	0.12	7.96

Table A2. Random Forest Regression(1D) prediction results. Note: groups 1–100 are the training set data, and groups 101–120 are the test set data.

Sample Number	Surface Roughness (μm)	Predicted Value (μm)	Error (%)	Descriptor
1	5.72	6.65	16%	3.45×10^{-3}
2	6.95	7.86	13%	4.15×10^{-3}
3	8.40	8.15	3%	4.31×10^{-3}
4	6.00	6.35	6%	3.28×10^{-3}
5	6.42	6.89	7%	3.59×10^{-3}
6	5.44	6.51	20%	3.38×10^{-3}
7	4.17	4.25	2%	2.09×10^{-3}
8	4.78	4.25	11%	2.08×10^{-3}
9	5.13	5.78	13%	2.96×10^{-3}
10	6.62	7.23	9%	3.79×10^{-3}
11	4.14	4.11	1%	2.01×10^{-3}
12	6.63	7.62	15%	4.01×10^{-3}
13	5.19	5.98	15%	3.07×10^{-3}
14	7.01	6.17	60%	3.18×10^{-3}
15	9.57	9.87	10%	5.30×10^{-3}
16	7.61	7.31	12%	3.83×10^{-3}
17	5.69	6.30	3%	3.25×10^{-3}
18	8.18	8.28	4%	4.38×10^{-3}
19	5.33	5.66	11%	2.89×10^{-3}
20	5.36	5.47	1%	2.78×10^{-3}
21	4.92	6.00	6%	3.08×10^{-3}
22	4.84	5.85	2%	3.00×10^{-3}
23	6.49	5.91	22%	3.03×10^{-3}
24	5.13	4.96	21%	2.49×10^{-3}
25	4.41	5.05	9%	2.54×10^{-3}
26	7.14	7.79	27%	4.11×10^{-3}
27	7.24	7.70	3%	4.06×10^{-3}
28	8.13	8.63	14%	4.59×10^{-3}
29	4.92	5.81	9%	2.97×10^{-3}
30	4.23	4.82	6%	2.41×10^{-3}
31	6.71	7.84	6%	4.14×10^{-3}
32	5.20	5.21	18%	2.63×10^{-3}
33	6.71	6.63	14%	3.44×10^{-3}
34	4.70	4.45	17%	2.20×10^{-3}
35	11.28	10.14	0%	5.45×10^{-3}
36	6.80	7.21	1%	3.78×10^{-3}
37	4.91	5.82	5%	2.98×10^{-3}
38	4.88	5.59	10%	2.85×10^{-3}
39	5.03	5.80	6%	2.97×10^{-3}
40	3.15	3.69	19%	1.77×10^{-3}
41	7.67	7.75	22%	4.09×10^{-3}
42	6.60	7.41	14%	3.89×10^{-3}
43	9.31	9.61	15%	5.15×10^{-3}
44	3.76	4.65	17%	2.31×10^{-3}
45	5.50	5.17	1%	2.61×10^{-3}
46	6.09	6.44	12%	3.34×10^{-3}
47	8.28	7.04	3%	3.68×10^{-3}
48	5.36	6.25	24%	3.23×10^{-3}
49	4.84	5.81	6%	2.98×10^{-3}
50	10.81	9.27	6%	4.95×10^{-3}
51	4.64	4.95	15%	2.49×10^{-3}
52	5.72	6.06	17%	3.12×10^{-3}
53	5.01	5.61	20%	2.86×10^{-3}

Table A2. *Cont.*

Sample Number	Surface Roughness (μm)	Predicted Value (μm)	Error (%)	Descriptor
54	4.23	3.96	14%	1.92×10^{-3}
55	4.23	3.93	7%	1.90×10^{-3}
56	8.92	9.71	6%	5.20×10^{-3}
57	5.65	6.71	12%	3.49×10^{-3}
58	7.20	7.57	6%	3.98×10^{-3}
59	5.26	5.29	7%	2.68×10^{-3}
60	5.14	6.12	26%	3.15×10^{-3}
61	8.24	7.99	9%	4.22×10^{-3}
62	6.67	7.04	19%	3.68×10^{-3}
63	3.65	4.74	5%	2.37×10^{-3}
64	5.64	6.57	1%	3.41×10^{-3}
65	8.22	7.96	19%	4.20×10^{-3}
66	10.42	9.30	3%	4.97×10^{-3}
67	7.77	7.38	6%	3.87×10^{-3}
68	4.71	4.86	30%	2.43×10^{-3}
69	7.54	6.79	17%	3.54×10^{-3}
70	6.42	5.69	3%	2.91×10^{-3}
71	5.47	5.84	11%	2.99×10^{-3}
72	4.90	5.82	5%	2.98×10^{-3}
73	5.81	5.75	3%	2.94×10^{-3}
74	5.48	6.43	10%	3.33×10^{-3}
75	7.64	7.20	11%	3.77×10^{-3}
76	7.14	7.73	7%	4.07×10^{-3}
77	5.34	6.58	19%	3.42×10^{-3}
78	4.91	6.02	1%	3.10×10^{-3}
79	4.94	4.90	17%	2.46×10^{-3}
80	8.37	6.06	6%	3.12×10^{-3}
81	9.46	8.71	8%	4.63×10^{-3}
82	7.10	5.56	23%	2.83×10^{-3}
83	7.51	6.71	23%	3.49×10^{-3}
84	7.70	7.73	1%	4.07×10^{-3}
85	9.92	10.02	8%	5.38×10^{-3}
86	4.37	5.62	11%	2.87×10^{-3}
87	9.59	9.94	0%	5.34×10^{-3}
88	4.06	3.86	1%	1.86×10^{-3}
89	8.98	7.78	29%	4.10×10^{-3}
90	9.88	9.76	4%	5.23×10^{-3}
91	7.84	6.54	5%	3.39×10^{-3}
92	6.47	5.72	0%	2.93×10^{-3}
93	8.15	8.79	13%	4.68×10^{-3}
94	7.11	8.01	1%	4.23×10^{-3}
95	6.54	6.77	12%	3.52×10^{-3}
96	5.51	5.84	8%	3.00×10^{-3}
97	7.36	7.19	13%	3.77×10^{-3}
98	5.37	5.73	4%	2.93×10^{-3}
99	4.70	5.06	6%	2.55×10^{-3}
100	4.77	4.87	2%	2.44×10^{-3}
101	8.11	7.04	9%	3.68×10^{-3}
102	7.38	5.80	7%	2.97×10^{-3}
103	7.31	8.75	8%	4.66×10^{-3}
104	6.77	7.93	2%	4.19×10^{-3}
105	6.84	6.80	16%	3.54×10^{-3}
106	10.01	9.21	1%	4.92×10^{-3}
107	10.18	8.65	15%	4.60×10^{-3}

Table A2. *Cont.*

Sample Number	Surface Roughness (μm)	Predicted Value (μm)	Error (%)	Descriptor
108	7.40	6.39	8%	3.31×10^{-3}
109	6.45	7.29	10%	3.82×10^{-3}
110	6.00	5.50	13%	2.80×10^{-3}
111	5.43	5.26	8%	2.66×10^{-3}
112	10.57	10.61	3%	5.71×10^{-3}
113	7.33	6.71	0%	3.49×10^{-3}
114	3.67	3.57	10%	1.70×10^{-3}
115	6.11	6.26	8%	3.23×10^{-3}
116	6.21	6.05	3%	3.11×10^{-3}
117	7.06	5.81	2%	2.98×10^{-3}
118	7.92	5.55	3%	2.83×10^{-3}
119	5.98	5.58	7%	2.85×10^{-3}
120	7.96	8.06	1%	4.26×10^{-3}

Table A3. Random Forest Regression(2D) prediction results. Note: groups 1–100 are the training set data, and groups 101–120 are the test set data.

Sample Number	Surface Roughness (μm)	Predicted Value (μm)	Error (%)	Descriptor 1	Descriptor 2
1	5.72	6.25	9%	2.14×10^{1}	-3.76×10^{2}
2	6.95	7.80	12%	2.06×10^{1}	-2.09×10^{2}
3	8.40	7.88	6%	2.12×10^{1}	-3.92×10^{2}
4	6.00	5.91	1%	2.14×10^{1}	-3.66×10^{2}
5	6.42	6.73	5%	2.08×10^{1}	-2.18×10^{2}
6	5.44	6.29	16%	2.12×10^{1}	-3.05×10^{2}
7	4.17	3.81	9%	2.17×10^{1}	-3.48×10^{2}
8	4.78	4.53	5%	2.21×10^{1}	-4.99×10^{2}
9	5.13	5.60	9%	2.10×10^{1}	-2.10×10^{2}
10	6.62	7.50	8%	2.06×10^{1}	-1.86×10^{2}
11	4.14	3.82	8%	2.17×10^{1}	-3.23×10^{2}
12	6.63	7.17	8%	2.11×10^{1}	-3.19×10^{2}
13	5.19	5.60	20%	2.16×10^{1}	-3.92×10^{2}
14	7.01	6.58	6%	2.18×10^{1}	-5.05×10^{2}
15	9.57	9.84	3%	2.03×10^{1}	-2.14×10^{2}
16	7.61	7.70	1%	2.05×10^{1}	-1.79×10^{2}
17	5.69	5.75	1%	2.12×10^{1}	-2.92×10^{2}
18	8.18	7.88	4%	2.09×10^{1}	-2.94×10^{2}
19	5.33	5.33	0%	2.12×10^{1}	-2.61×10^{2}
20	5.36	5.55	4%	2.18×10^{1}	-4.64×10^{2}
21	4.92	5.45	11%	2.13×10^{1}	-3.11×10^{2}
22	4.84	5.30	10%	2.14×10^{1}	-3.17×10^{2}
23	6.49	6.42	1%	2.18×10^{1}	-5.16×10^{2}
24	5.13	5.78	13%	2.19×10^{1}	-5.11×10^{2}
25	4.41	4.45	1%	2.13×10^{1}	-2.54×10^{2}
26	7.14	8.14	14%	2.04×10^{1}	-1.73×10^{2}
27	7.24	7.35	2%	2.08×10^{1}	-2.59×10^{2}
28	8.13	9.02	11%	2.03×10^{1}	-1.84×10^{2}
29	4.92	6.04	23%	2.08×10^{1}	-1.72×10^{2}
30	4.23	4.64	10%	2.19×10^{1}	-4.34×10^{2}
31	6.71	7.59	13%	2.07×10^{1}	-2.36×10^{2}
32	5.20	4.76	8%	2.13×10^{1}	-2.66×10^{2}
33	6.71	6.52	3%	2.08×10^{1}	-2.05×10^{2}

Table A3. *Cont.*

Sample Number	Surface Roughness (μm)	Predicted Value (μm)	Error (%)	Descriptor 1	Descriptor 2
34	4.70	4.27	9%	2.12×10^1	-1.94×10^2
35	11.28	10.32	9%	2.01×10^1	-1.85×10^2
36	6.80	6.89	1%	2.13×10^1	-3.82×10^2
37	4.91	5.52	13%	2.14×10^1	-3.20×10^2
38	4.88	5.29	8%	2.11×10^1	-2.35×10^2
39	5.03	5.54	10%	2.11×10^1	-2.28×10^2
40	3.15	3.54	12%	2.20×10^1	-4.06×10^2
41	7.67	7.49	2%	2.13×10^1	-3.94×10^2
42	6.60	7.17	9%	2.08×10^1	-2.42×10^2
43	9.31	9.78	5%	2.02×10^1	-1.89×10^2
44	3.76	4.75	26%	2.17×10^1	-3.82×10^2
45	5.50	5.69	3%	2.20×10^1	-5.20×10^2
46	6.09	6.18	2%	2.10×10^1	-2.35×10^2
47	8.28	7.97	4%	2.04×10^1	-1.50×10^2
48	5.36	5.77	8%	2.13×10^1	-3.11×10^2
49	4.84	5.58	15%	2.16×10^1	-3.89×10^2
50	10.81	10.36	4%	1.99×10^1	-1.39×10^2
51	4.64	4.87	5%	2.11×10^1	-1.89×10^2
52	5.72	6.00	5%	2.13×10^1	-3.38×10^2
53	5.01	5.12	2%	2.15×10^1	-3.42×10^2
54	4.23	4.64	10%	2.22×10^1	-5.39×10^2
55	4.23	3.30	22%	2.17×10^1	-3.11×10^2
56	8.92	9.38	5%	2.05×10^1	-2.52×10^2
57	5.65	6.75	19%	2.08×10^1	-2.11×10^2
58	7.20	7.31	1%	2.12×10^1	-3.75×10^2
59	5.26	5.74	9%	2.17×10^1	-4.25×10^2
60	5.14	5.98	16%	2.09×10^1	-2.03×10^2
61	8.24	7.55	8%	2.09×10^1	-2.99×10^2
62	6.67	6.66	0%	2.13×10^1	-3.69×10^2
63	3.65	4.34	19%	2.17×10^1	-3.51×10^2
64	5.64	6.39	13%	2.15×10^1	-4.12×10^2
65	8.22	7.55	8%	2.11×10^1	-3.36×10^2
66	10.42	9.33	10%	2.03×10^1	-2.09×10^2
67	7.77	8.15	5%	2.04×10^1	-1.49×10^2
68	4.71	4.29	9%	2.17×10^1	-3.62×10^2
69	7.54	7.55	0%	2.05×10^1	-1.49×10^2
70	6.42	6.51	1%	2.06×10^1	-1.40×10^2
71	5.47	5.24	4%	2.15×10^1	-3.33×10^2
72	4.90	6.00	23%	2.16×10^1	-4.17×10^2
73	5.81	6.83	18%	2.05×10^1	-1.30×10^2
74	5.48	6.12	12%	2.10×10^1	-2.29×10^2
75	7.64	7.04	8%	2.08×10^1	-2.21×10^2
76	7.14	7.56	6%	2.13×10^1	-4.13×10^2
77	5.34	6.22	16%	2.10×10^1	-2.56×10^2
78	4.91	5.49	12%	2.13×10^1	-2.86×10^2
79	4.94	4.28	13%	2.16×10^1	-3.16×10^2
80	8.37	7.75	7%	2.19×10^1	-6.04×10^2
81	9.46	9.19	3%	2.03×10^1	-1.75×10^2
82	7.10	6.72	5%	2.20×10^1	-5.74×10^2
83	7.51	6.49	14%	2.12×10^1	-3.36×10^2
84	7.70	7.46	3%	2.08×10^1	-2.57×10^2
85	9.92	9.64	3%	2.05×10^1	-2.81×10^2
86	4.37	5.46	25%	2.10×10^1	-2.01×10^2
87	9.59	9.74	1%	2.04×10^1	-2.38×10^2

Table A3. *Cont.*

Sample Number	Surface Roughness (μm)	Predicted Value (μm)	Error (%)	Descriptor 1	Descriptor 2
88	4.06	3.64	10%	2.19×10^1	-3.82×10^2
89	8.98	8.96	0%	2.02×10^1	-1.34×10^2
90	9.88	10.11	2%	2.01×10^1	-1.76×10^2
91	7.84	7.52	4%	2.04×10^1	-1.43×10^2
92	6.47	6.97	8%	2.19×10^1	-5.53×10^2
93	8.15	8.77	8%	2.05×10^1	-2.18×10^2
94	7.11	7.97	12%	2.06×10^1	-2.09×10^2
95	6.54	6.28	4%	2.11×10^1	-2.75×10^2
96	5.51	5.54	1%	2.11×10^1	-2.42×10^2
97	7.36	6.69	9%	2.11×10^1	-3.15×10^2
98	5.37	5.43	1%	2.11×10^1	-2.19×10^2
99	4.70	4.44	6%	2.14×10^1	-2.60×10^2
100	4.77	4.55	5%	2.16×10^1	-3.45×10^2
101	8.11	7.02	8%	2.07×10^1	-2.01×10^2
102	7.38	7.02	5%	2.18×10^1	-5.38×10^2
103	7.31	8.34	14%	2.09×10^1	-3.32×10^2
104	6.77	7.49	11%	2.10×10^1	-3.14×10^2
105	6.84	6.59	4%	2.13×10^1	-3.60×10^2
106	10.01	9.45	6%	2.02×10^1	-1.84×10^2
107	10.18	9.44	7%	2.01×10^1	-1.53×10^2
108	7.40	7.96	8%	2.03×10^1	-1.18×10^2
109	6.45	6.91	7%	2.09×10^1	-2.52×10^2
110	6.00	5.64	6%	2.17×10^1	-4.27×10^2
111	5.43	5.75	6%	2.17×10^1	-4.50×10^2
112	10.57	10.35	2%	2.02×10^1	-2.30×10^2
113	7.33	6.97	5%	2.15×10^1	-4.43×10^2
114	3.67	3.98	8%	2.23×10^1	-5.12×10^2
115	6.11	6.04	1%	2.12×10^1	-3.05×10^2
116	6.21	5.77	7%	2.12×10^1	-2.87×10^2
117	7.06	7.15	1%	2.18×10^1	-5.34×10^2
118	7.92	7.08	11%	2.19×10^1	-5.77×10^2
119	5.98	5.53	8%	2.14×10^1	-3.38×10^2
120	7.96	7.67	4%	2.11×10^1	-3.39×10^2

References

1. Debroy, T.; Wei, H.L.; Zuback, J.S.; Mukherjee, T.; Elmer, J.W.; Milewski, J.O.; Beese, A.M.; Wilson-Heid, A.; De, A.; Zhang, W. Additive manufacturing of metallic components—Process. structure and properties. *Prog. Mater. Sci.* **2018**, *12*, 112–224. [CrossRef]
2. Wang, K.; Xie, G.Q.; Xiang, J.Y.; Li, T.; Peng, Y.; Wang, J.; Zhang, H.H. Materials selection of 3D printed polyamide-based composites at different strain rates: A case study of automobile front bumpers. *J. Manuf. Process.* **2022**, *84*, 1449–1462. [CrossRef]
3. Yan, H.; Zhang, J.Z.P.L.; Yu, Z.S.; Li, C.G.; Xu, P.Q.; Lu, Y.L. Laser cladding of Co-based alloy/TiC/CaF2 self-lubricating composite coatings on copper for continuous casting mold. *Surf. Coat. Technol.* **2013**, *232*, 362–369. [CrossRef]
4. Ponnusamy, P.; Rashid, R.A.R.; Masood, S.H.; Ruan, D.; Palanisamy, S. Mechanical Properties of SLM-Printed Aluminium Alloys: A Review. *Materials* **2020**, *13*, 4301. [CrossRef]
5. Cottam, R.; Palanisamy, S.; Jarvis, T.; Cuiuri, D.; Leary, M.; Singh, M.; Rashid, R.A.R. Post-processing and machining of Ti6Al4V coupons fabricated using various metal additive manufacturing technologies. *Compr. Mater. Process.* **2024**, *9*, 132–147. [CrossRef]
6. Gao, C.; Tang, H.; Zhang, S.; Ma, Z.; Bi, Y.; Rao, J.-H. Process Optimization for Up-Facing Surface Finish of AlSi10Mg Alloy Produced by Laser Powder Bed Fusion. *Metals* **2022**, *12*, 2053. [CrossRef]
7. Xie, X.Y.; Ho, J.W.K.; Murphy, C.; Kaiser, G.; Xu, B.W.; Chen, T.Y. Testing and validating machine learning classifiers by metamorphic testing. *J. Syst. Softw.* **2011**, *84*, 544–558. [CrossRef]
8. Fotovvati, B.; Chou, K. Build surface study of single-layer raster scanning in selective laser melting: Surface roughness prediction using deep learning. *Manuf. Lett.* **2022**, *33*, 701–711. [CrossRef]
9. Li, Z.X.; Zhang, Z.Y.; Shi, J.C.; Wu, D.Z. Prediction of surface roughness in extrusion-based additive manufacturing with machine learning. *Robot. Comput. Integr. Manuf.* **2019**, *57*, 488–495. [CrossRef]

10. Yang, D.H.; MA, L.; Huang, W.D. Component's Surface Quality Predictions by Laser Rapid Forming Based on Artificial Neural Networks. *Chin. J. Lasers* **2011**, *38*, 83–88. [CrossRef]
11. Deb, J.; Chowdhury, S.; Ali, N.M. An investigation of the ensemble machine learning techniques for predicting mechanical properties of printed parts in additive manufacturing. *Decis. Anal. J.* **2024**, *12*, 100492. [CrossRef]
12. Chen, H.; Yaseer, A.; Zhang, Y. Top Surface Roughness Modeling for Robotic Wire Arc Additive Manufacturing. *J. Manuf. Mater. Process.* **2022**, *6*, 39. [CrossRef]
13. Gogulamudi, B.; Bandlamudi, R.K.; Bhanavathu, B.; Guttula, V.S.K. A Prediction Model for Additive Manufacturing of AlSi10Mg Alloy. *Trans. Indian Inst. Met.* **2023**, *76*, 571–579. [CrossRef]
14. Loreti, D.; Visani, G. Parallel approaches for a decision tree-based explainability algorithm. *Future Gener. Comput. Syst.* **2024**, *158*, 308–322. [CrossRef]
15. Antoniadis, A.; Lambert-Lacroix, S.; Poggi, J.M. Random forests for global sensitivity analysis: A selective review. *Reliab. Eng. Syst. Saf.* **2020**, *206*, 107312. [CrossRef]
16. Dorian, V.; Louis, G.; Elodie, C.; Louise, T.-M.; Sébastien, D. Machine Learning Based Fault Anticipation for 3D Printing. *IFAC-PapersOnLine* **2023**, *56*, 2927–2932. [CrossRef]
17. Lu, Y.X.; Rai, R.W.; Nitin, N. Image-based assessment and machine learning-enabled prediction of printability of polysaccharides-based food ink for 3D printing. *Food Res. Int.* **2023**, *173*, 113384. [CrossRef]
18. Huang, H.; Liu, J.H.; Liu, S.L.; Wu, T.Y.; Jin, P. A method for classifying tube structures based on shape descriptors and a random forest classifier. *Measurement* **2020**, *158*, 107705. [CrossRef]
19. Huang, J.W.; Zhang, H.O.; Li, R.S.; Zhao, X.S.; Lin, H.; Zhai, W.Z.; Wang, G.L.; Fu, Y.H. Hybrid in-situ hot rolling and wire arc additive manufacturing of Al-Si alloy: Microstructure. mechanical properties and strengthening mechanism. *J. Manuf. Process.* **2024**, *127*, 328–339. [CrossRef]
20. Bisht, M.S.; Gaur, V.; Singh, I.V. On mechanical properties of L-PBF Al–Si alloy: Role of heat treatment-induced evolution of silicon morphology. *Mater. Sci. Eng. A* **2022**, *858*, 144157. [CrossRef]
21. Olakanmi, E.O. Selective laser sintering/melting (SLS/L-PBF) of pure Al; Al–Mg, and Al–Si powders: Effect of processing conditions and powder properties. *J. Mater. Process. Technol.* **2013**, *213*, 1387–1405. [CrossRef]
22. Pawlus, P.; Reizer, R.; Wieczorowski, M.; Krolczyk, G.M. Study of surface texture measurement errors. *Measurement* **2023**, *210*, 112568. [CrossRef]
23. Podulka, P.; Macek, W.; Branco, R.; Kubit, A. Laser-textured cross-hatched surface topography analysis with evaluation of high-frequency measurement noise. *Measurement* **2024**, *235*, 114988. [CrossRef]
24. Brudler, S.; Medvedev, A.E.; Pandelidi, C.; Piegert, S.; Illston, T.; Qian, M.; Brandt, M. Systematic investigation of performance and productivity in Laser Powder Bed Fusion of Ti6Al4V up to 300 µm layer thickness. *J. Mater. Process. Technol.* **2024**, *330*, 118450. [CrossRef]
25. Wang, Y.H.; Hu, Q.; Zhang, J.H.; Liu, Y.J.; Sheng, Y.W.; Zhao, X.M. Influencing factors on the tensile properties of selective laser melting 3D printing AlSi10Mg. *Powder Metall. Technol.* **2022**, *40*, 152–158. [CrossRef]
26. Gong, D.L.; Bian, H.K.; Pan, D.; Xu, S.H.; Yang, X.; Yang, H.P. Research advances in powder bed fusion additive manufacturing AlSi10Mg alloy. *Chin. J. Nonferrous Met.* **2024**, *34*, 1091–1112. [CrossRef]
27. Leis, A.; Traunecker, D.; Weber, R.; Graf, T. Tuning the Hardness of Produced Parts by Adjusting the Cooling Rate during Laser-Based Powder Bed Fusion of AlSi10Mg by Adapting the Process Parameters. *Metals* **2022**, *12*, 2000. [CrossRef]
28. Zhang, X.J.; Chu, D.M.; Zhao, X.Y.; Gao, C.Y.; Lu, L.X.; He, Y.; Bai, W.J. Machine learning-driven. *Appl. Mater. Today* **2024**, *39*, 102306. [CrossRef]
29. Geng, S.Y.; Mei, L.; Cheng, B.Y.; Luo, Q.L.; Xiong, C.; Long, W.J. Revolutionizing 3D concrete printing: Leveraging RF model for precise printability and rheological prediction. *J. Build. Eng.* **2024**, *88*, 109127. [CrossRef]
30. Zhang, W.H.; Ma, H.L.; Zhang, Q.; Fan, S.Q. Prediction of powder bed thickness by spatter detection from coaxial optical images in selective laser melting of 316L stainless steel. *Mater. Des.* **2022**, *213*, 110301. [CrossRef]
31. Lacy, F.; Ruiz-Reyes, A.; Brescia, A. Machine learning for low signal-to-noise ratio detection. *Pattern Recognit. Lett.* **2024**, *179*, 115–122. [CrossRef]